Chapter 7

High-Aspect-Ratio Metallic Nanostructures for Transparent Electrodes

Joong-Mok Park,[a,*] Xinyu Liu,[a] Wai Leung,[a] Kristen Constant,[a,b] Alan Russell,[a,b] and Kai-Ming Ho[a,c]

[a] *Ames Laboratory — U.S. DOE, Ames, Iowa 50011, USA*

[b] *Department of Material Science, Iowa State University, Ames, Iowa 50011, USA*

[c] *Department of Physics and Astronomy, Ames, Iowa 50011, USA*

*joongmok@iastate.edu

Metallic nanowire arrays having high optical transmission and electric conductivity show promise for use as transparent electrodes. Transparent electrodes require high transmission of visible light and good electrical conductivity for charge transfer. High-aspect-ratio metallic nanowires for transparent electrode applications can be fabricated by e-beam angular deposition on polymer templates. These polymer templates are made with interference holography and nanoimprinting using a polydimethylsiloxane (PDMS) mold. The details of the fabrication processes including interference holography, micro-transfer molding, nanoimprint, and shadow angle depositions will be discussed.

Vistas in Nanofabrication
Edited by Faiz Rahman
Copyright © 2013 Pan Stanford Publishing Pte. Ltd.
ISBN 978-981-4364-56-0 (Hardcover), 978-981-4364-57-7 (eBook)
www.panstanford.com

7.1 Introduction

Semiconducting and metallic nanowires have many interesting physical, electrical, optical, and chemical properties due to their simple nature and one-dimensional geometry [1]. Their mechanical and electrical properties depend on the average grain size achieved during their growth. Grain growth mechanisms are well-studied for thin films and bulk materials, but there are few studies on nanowires [2,3]. The average grain size of metallic nanowires and thin films is generally smaller than that of bulk but can be increased by thermal annealing. In our work, metallic nanowires of Ti, Au, and Al were fabricated using physical deposition on polymer templates. The dimensions and grain growth of the nanowires were monitored *in situ* during the annealing process by transmission electron microscopy (TEM). Optical and electrical properties of the high-aspect-ratio metallic nanowire arrays were measured. Metallic or metal oxide thin films are currently used as transparent electrodes, but the thicknesses are constrained by the competing requirements of maximizing optical transparency and electrical conductivity. Typically, thicker films have desirable higher electric conductivity but transmission decreases exponentially due to increased radiation absorption. To decouple electric conductivity and optical transparency, tall and thin (high aspect ratio) metallic nanowires were proposed and fabricated [4]. The high-aspect metallic nanowires have optical and electrical properties similar to indium tin oxide (ITO) and have potential for use as transparent electrodes in many practical optical devices.

7.2 Fabrication of Nanowire Using Polymer Templates

Nanowires were made by e-beam assisted physical vapor deposition of metal on polymer templates. The polymer templates were made either with interference lithography or through nanoimprinting.

7.2.1 Polymer Template Fabrication

Photoresist gratings were fabricated with laser interference holography [5,6] and photosensitive materials (photoresist), which selectively react upon exposure to light, typically ultraviolet.

Instead of a photo mask, the interference of coherent beams is used to construct one- or two-dimensional periodic structures. The interference is the superposition of two coherent beams, the sum of the electric fields, as illustrated in Fig. 7.1. The intensity of the interference is the time-averaged value during the exposure and is simplified as

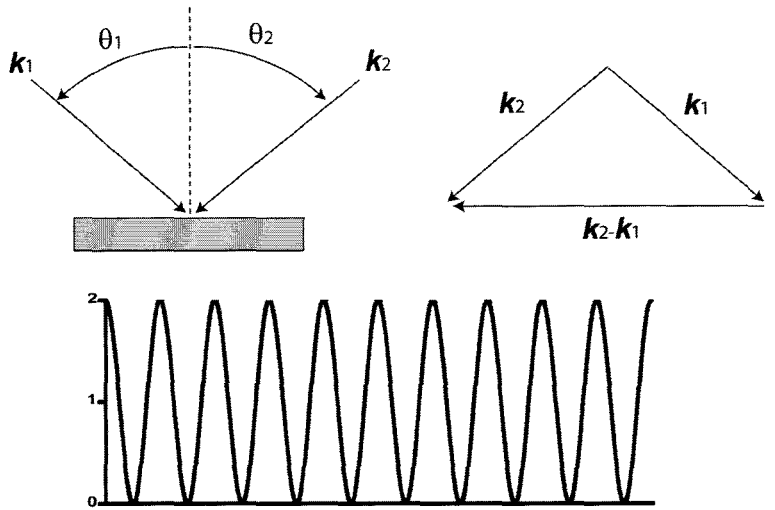

Figure 7.1 Interference of two coherent beams at two incidence angles and the intensity of the interference along the sample surface.

$$I = \langle |E_1 + E_2|^2 \rangle = I_0[1 + \cos(k_2 - k_1)x], \tag{7.1}$$

where E_1 and E_2 are time-dependent electric fields and k_1 and k_2 are wave numbers.

The pitch (P) of the constructive and destructive interference patterns is a function of the laser wavelength (λ) and the angle of incidence (θ) from the normal: $P = \lambda/(\sin(\theta_2) - \sin(\theta_1))$. Because the intensity of the interference is sinusoidal, a periodic line grating forms in the photoresist. An Ar-ion laser (λ = 364 nm) was used as the coherent light source, and the pitch can be adjusted to $\lambda/2$ by changing the incidence angles. The exposed area is determined by the size of optical components and the coherence length of the laser. Large samples were made by expanding the beams with a UV objective lens and exposed at 2 m from the focal point of the lens. A Lloyd's mirror setup was used as shown in Fig. 7.2a [6].

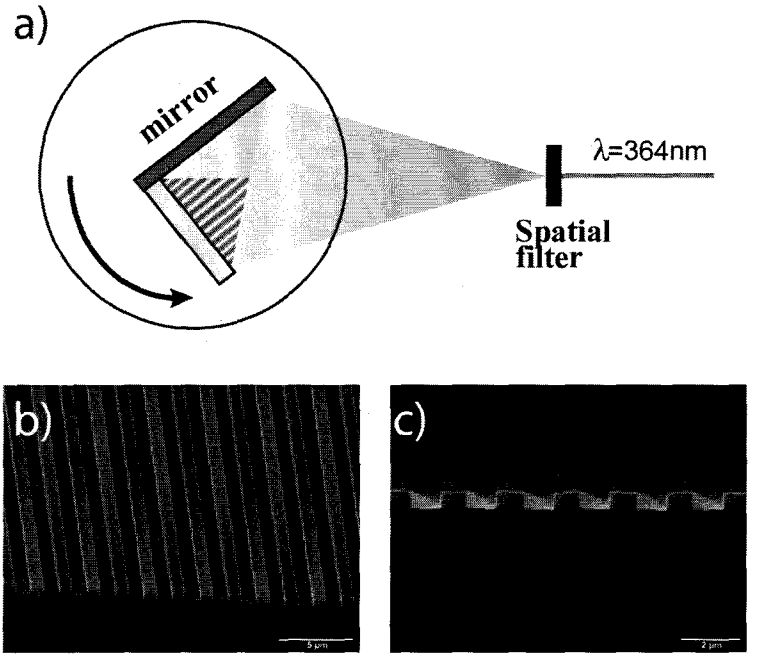

Figure 7.2 (a) Schematic diagram of the interference lithography setup with the Lloyd's mirror configuration. (b) SEM image of photoresist grating made by interference lithography on a silicon substrate. (b) Cross-sectional image of the photoresist.

One reflected beam from a mirror and the other one from the objective lens created the interference pattern. The mirror was attached at right angle to the sample and the assembly was rotated together to maintain the same incidence angles. Following the laser exposure of the photoresist, the sample was developed, leaving a grating structure of photoresist on the substrate as shown in Fig. 7.2b,c. Note that photoresists structures have a rectangular cross section even though the intensity of the light is sinusoidal.

Other well-known methods for making nanostructures with polymer materials are nanoimprinting [7,8] and micro-transfer molding [9]. Here, PDMS is used to replicate the inverse structure of the original master pattern. A second polymer, polyurethane (PU), is used to duplicate the inverse structure of the PDMS mold. The PU then attains the same structure as the original master pattern through double inversion.

7.2.2 Metal Deposition

After polymer templates were made, various metals were deposited on the templates by e-beam evaporation. A deposition rate of 1 Å/s and a pressure below 10^{-6} Torr were maintained during the depositions. Because the distance between the e-beam source and the specimen was 1 m, a distance far enough for line-of-sight deposition, metals were deposited only on the tops and the bottoms of the grating, leaving the sidewall of the grating surfaces uncoated as shown in Fig. 7.3a,b. Thus, two sets of nanowires were produced; one set adhering to the substrate and a second set adhering to the tops of the polymer grating. After deposition, the polymer templates can be dissolved with a photoresist remover (Microchem Inc., Remover PG), releasing the deposited metal nanowires atop the grating into the rinse solution, isopropyl alcohol. The metallic nanowires in solution were then dropped onto a flat substrate and dried in vacuum. The collected nanowires were slightly curled as shown in Fig. 7.4a,b. Half of the metallic nanowires, those that were deposited in the channels between the polymer remained on the substrate even after polymer removal as seen in Fig. 7.4c. Al, Au, and Ti nanowires have smooth surfaces compared to that of Pb nanowires. There was no substrate heating during the deposition except the heat radiation from the source. The high mobility of Pb atoms on the substrate during the initial grain growth stage results in a large grained structure as seen in Fig. 7.4d. For this reason, Pb nanowires cannot be obtained with this method. Additionally, they easily oxidize after a short period of exposure in air.

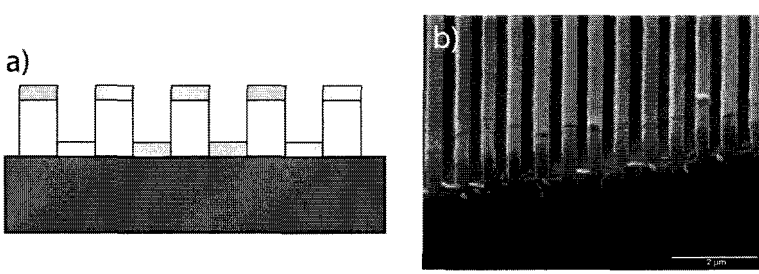

Figure 7.3 (a) Schematic diagram of metal deposition on the polymer template at normal angle. (b) SEM image of 100 nm-thick Al coated on the top and the channels of the photoresist.

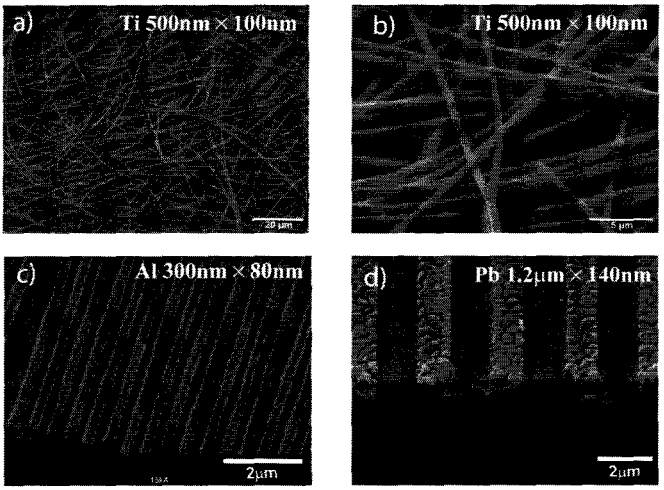

Figure 7.4 (a, b) SEM images of nanowires collected from the solvent used for dissolving photoresist. (c) Al, and (d) Pb nanowires on the substrate after photoresist is removed.

7.3 Characterization of Nanowires

7.3.1 Transmission Electron Microscopy

Once the metal nanowires were made, these were transferred onto a graphite mesh for TEM observations as shown in Fig. 7.5a. The nanowires were broken into lengths of a few microns by ultrasonic agitation for 1 minute in isopropyl alcohol to avoid self-folding. Then the broken nanowires in solvent were dropped onto a graphite mesh and suspended by vacuum-assisted drying. Also, a metal thin film having voids was made to support the ordered metal nanowires instead of using the graphite mesh. Cu thin films were coated by electro-deposition onto the nanowires with the templates on the substrate, and then a hole was selectively etched out of the Cu, leaving metallic nanowires bridging over these holes after separating the Cu thin film from the substrate as shown in Fig. 7.5b. These metallic nanowires were suspended across the gap and adhered to the free-standing Cu substrate on either side of the gap. This allowed the nanowires to span a window in the substrate so an electron beam could pass through the nanowires. In this way the nanowires can be imaged *in situ* by TEM.

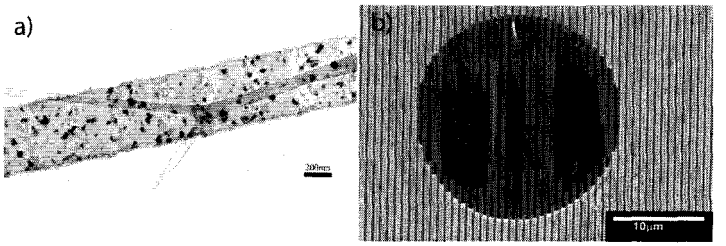

Figure 7.5 (a) TEM micrograph of a 400 nm-wide and 100 nm-thick Al nanowire suspended on a Y-shaped graphite mesh. Some Al grains are oriented so as to appear dark in this image. (b) SEM image of Ti metal nanowires suspended across Cu film having a circular hole.

TEM observation of deposited nanowires shown in Fig. 7.6 shows that the metal is thin enough (~100 nm) to be electron transparent to the 200–300 kV beam energies used in TEM microscopes. The as-sputtered Ti and Al nanowires shown in Fig. 7.6a,c have undesirably small average grain sizes. Such small grains are typical of sputtered films. In addition, dislocation generation and multiplication would be facilitated by larger grains. The average grain sizes were about a few nm for Ti and 10–20 nm for Al nanowires as-grown. Their average grain sizes were increased after annealing, but large or bamboo-like grains were not observed. To check the grain growth over a long period of time, 80 nm-thick Au nanowire samples were placed in an ultra-high vacuum chamber. Au nanowires were annealed for 100 hours at 300°C and at a pressure below 4×10^{-8} Torr. Their average grain size is close to that annealed at 600°C *in situ* for 14 minutes as seen in Fig. 7.7b–d.

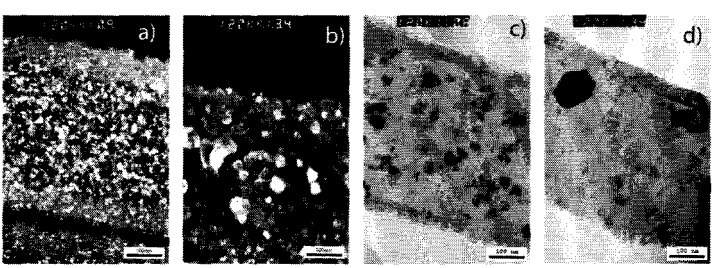

Figure 7.6 TEM micrograph of a 100 nm-thick layer of (a) Ti nanowires before annealing and (b) after annealing at 950°C for 10 minutes. TEM images of (c) Al nanowires before annealing and (d) after annealing at 600°C for 160 minutes.

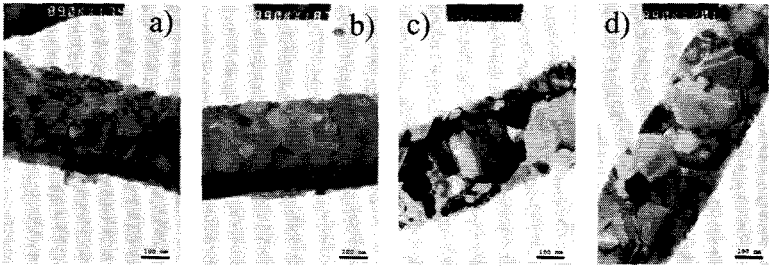

Figure 7.7 TEM micrograph of a 80 nm-thick Au nanowires sample (a) before annealing and (b) after *in situ* annealing at 600°C for 14 minutes. (c, d) Au nanowires after annealing at 300°C for 100 hours under ultra high vacuum. The pressure was below 4×10^{-8} Torr during annealing.

7.3.2 *In situ* Grain Growth

Larger grains might be produced by long, high-temperature vacuum anneals to promote grain growth to coarsen the grains of the nanowires. However, previous work on metallic thin films suggests that post-deposition grain coarsening may also result in undesirable effects such as pitting of the surface or otherwise compromising the sample geometry. An alternative approach is to modify metal deposition conditions to control the grain structure. The control of deposition conditions requires modification of the sputtering system to include a rotating, temperature-controlled sample stage, ideally with both heating and cooling capabilities. Figure 7.8 shows TEM images of 100 nm-thick Al nanowires taken during *in situ* annealing at 600°C. A large grain appears abruptly through the merging of two adjacent grains.

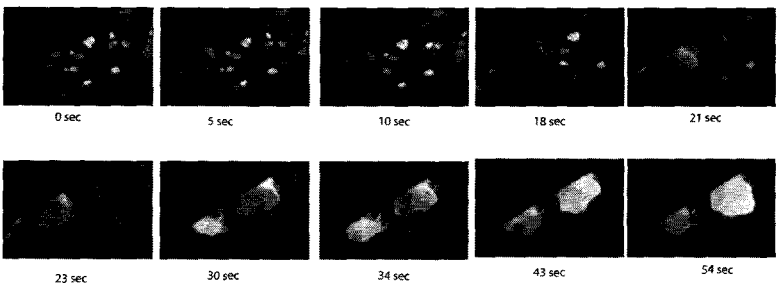

Figure 7.8 TEM micrograph of a 100 nm-thick Al nanowire during *in situ* annealing process at 600°C.

For gold nanowires, we obtained bamboo-like grain structures after *in situ* heating at 700°C for ~1 hour as seen in Fig. 7.9a,b. The diffraction pattern of the electron beam focused on a domain confirmed the existence of the single grain as shown in Fig. 7.9c. This method provided us an opportunity to study the dislocation behavior and allowed us to control the electrical and mechanical properties of nanowires by manipulating the grain structure and grain boundaries.

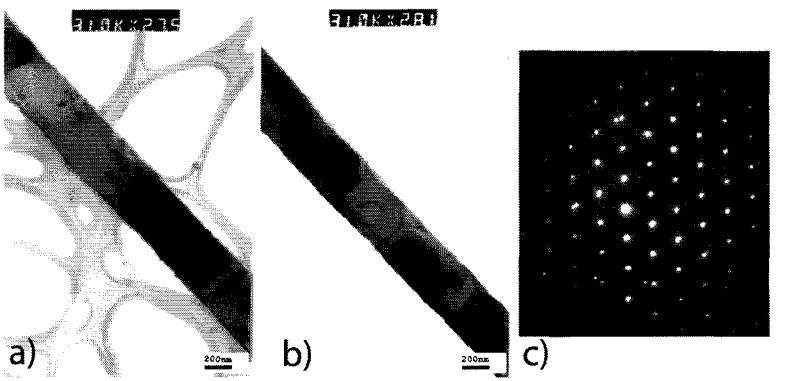

Figure 7.9 (a, b) TEM images of gold nanowires after *in situ* heating at 700°C for ~1 hour. The bamboo-like grain structure is evident. (c) Electron diffraction pattern showing a single grain.

7.4 Shadow Angle Deposition

7.4.1 Shadow Deposition of Metal Nanowires

Figure 7.10a shows a schematic diagram of a shadow-angle-deposition technique [10–12]. The polymer is used as the deposition template and also as a shadow mask. The thickness of the metal on the top and sidewalls is determined by the height of the polymer and the incidence angle. The top thickness is $t\cos(\theta)$, and the sidewall thickness is $t\sin(\theta)$, where t is the normal deposition thickness. For low angles, such as 15°, as in Fig. 7.10b, the top metal coating is thick, while the sidewall is thin. With a 45° angle deposition, the top and sidewall have the same thickness as shown in the inset of Fig. 7.10b.

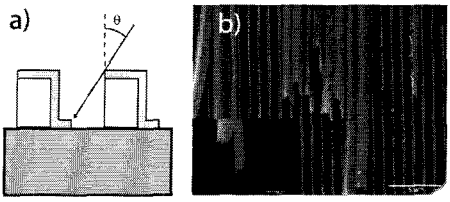

Figure 7.10 Shadow angle deposition and SEM image of Ti nanowires at 15° angle. Inset shows Ti nanowires deposited at 45°.

7.4.2 High-Aspect-Ratio Metallic Structures by Ar Etching

The angular deposition technique can be used to avoid deposition in the polymer channels by shadowing. The metal deposited on top can be removed by physical etching with high-energy Ar ions. The high-energy Ar etches the top, leaving well-aligned high-aspect-ratio metallic structures deposited on the sidewalls as shown in Fig. 7.11a. With controlled etching conditions, the polymer templates can be left intact to provide mechanical support for the high-aspect-ratio nanowires as seen in Fig. 7.11b [4]. Metals were also deposited on both side walls by two depositions at 45° and -45° as seen in Fig. 7.11b. Electron transmission is enhanced by removal of the top metal coating of the polymer, but there is significant diffraction from the polymer grating. This diffraction can be reduced by encapsulation of the polymer with a material having the same refractive index. The electrical conductivity is better than that of ITO, which is often used in displays and photovoltaic applications. This architecture has the potential to be used as a replacement for transparent electrodes without the use of indium, which suffers from high cost and diminishing supplies.

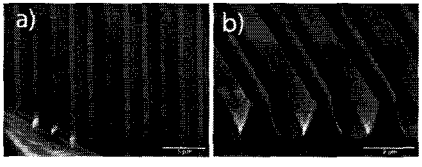

Figure 7.11 (a) After Ar plasma etching the top Au layer deposited on the polymer, and the polymer template were etched away, leaving single sidewalls on the substrate. (b) Etched top of the gold having double sidewalls with Ar ion milling. The polymer templates (PU) were partially etched and remained between the metals.

7.4.3 Electrical and Optical Properties

Electrical conductivity measurement of a single nanowire would require very small electrodes [13–16]. However, measuring a large number of nanowires gives more accurate values and does not require nanometer-scale electrodes or actuators. Simply adding millimeter-wide contact pads of Ag epoxy or thin film metal deposition allows the measurement of resistivity. The contact resistance between nanowires and the contact pad is much less than 1 ohm. A simple two-point measurement is sufficient to measure the resistance of nanowires. Samples with two different heights (300 nm and 1400 nm) were fabricated with PU polymer templates with nanoimprinting [4]. A 40 nm-thick Au layer was deposited on both sides of the polymer, and the top was removed by Ar ion milling. The measured resistance was 16 ohm for 1400 nm tall and 40 nm wide Au nanowires array and 52 ohm for 300 nm tall and 40 nm wide Au nanowires array. The length of the nanowires was 2.5 cm and a total of 4×10^4 nanowires measured at the same time. The typical resistance of 150 nm ITO-coated glass having the same dimensions is 30 ohms.

The optical transmission of the grating structures exhibits diffraction orders dependent on the dimensions of the gratings including pitch and height. Such diffraction can be utilized in various applications. The optical transmissions of the high-aspect-ratio metallic nanowires with PU templates were measured at normal incidence angle after the top Au layer was removed. The specular transmission is the transmitted intensity of the 0^{th} order diffracted light, and the total transmission is the integrated transmitted intensity of all diffracted orders. The total transmission was measured by placing the sample on a 3 mm opening of the input port of a 75 mm diameter integrating sphere. A fiber-coupled spectrometer (Ocean optics S2000) analyzed the transmission spectrum. As seen in Fig. 7.12, specular transmissions are increased by encapsulation, which indicates that the higher-order diffractions are suppressed. This is essential for some applications such as smart windows, displays, or back-lighting. Also, there is a slight (few %) enhancement of total transmission after encapsulation. This is due to the over-etched polymer being filled by encapsulated materials.

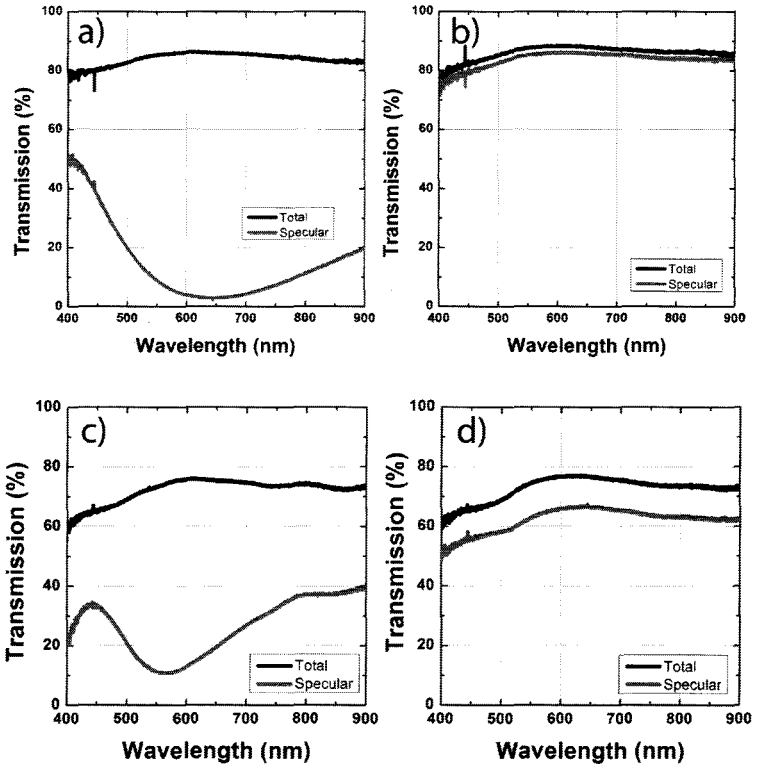

Figure 7.12 Optical transmission of high-aspect-ratio Au nanowire array after removal of the Au deposited on the top of the polymer. (a) The height = 300 nm and width = 40 nm before and (b) after encapsulation. (c) The height = 1400 nm and width = 40 nm before and (d) after encapsulation. See also Color Insert.

7.5 Conclusions

In summary, we fabricated metallic nanowires with laser interference holography, nanoimprint, and e-beam angular metal depositions. This fabrication method can produce well-defined, rectangular cross-sectional nanowires with dimensions of a few cm in length and submicron width. Structural properties of metallic nanowires were examined with SEM and TEM. The high-aspect-ratio metallic nanowires show both high optical transmission and high electrical conductivity after the metals deposited on top were

removed. Encapsulation of the nanowires suppressed the high-order diffractions.

Acknowledgments

This work was supported by the Director for Energy Research, Office of Basic Energy Sciences. The Ames Laboratory is operated for the U.S. Department of Energy by Iowa State University under contract No. W-7405-Eng-82.

References

1. Pauzauskie, P.J., and Yang, P. (2006), Nanowire photonics, *Mater. Today*, **9**, pp. 36–45.
2. Thompson, C.V. (1990), Grain growth in thin films, *Annu. Rev. Mater. Sci.*, **20**, pp. 245–268.
3. Fayad, W., Thompson, C.V., and Frost, H.J. (1999), Steady-state grain-size distributions resulting from grain growth in two dimensions, *Scripta Mater.*, **40**, pp. 1199–1204.
4. Kuang, P., Park, J.M., Leung, W., Mahadevapuram, R.C., Nalwa, K.S., Kim, T.G., Chaudhary, S., Ho, K.M., and Constant K. (2011), A new architecture for transparent electrodes: relieving the trade-off between electrical conductivity and optical transmittance. *Adv. Mater.*, 23, 2469–2473.
5. Prenen, A.M., Werf, J.C.A., Bastiaansen, C.W.M., and Broer D.J. (2009), Monodisperse, polymeric nano and microsieves produced with interference holography, *Adv. Mater.*, **21**, pp. 1751–1755.
6. Park, J.M., Nalwa, K.S., Leung, W., Constant, K., Chaudhary, S., and Ho, K.M. (2010), Fabrication of metallic nanowires and nanoribbons using laser interference lithography and shadow lithography, *Nanotechnology*, **21**, 215301 (6pp).
7. Guo, L.J. (2006), Nanoimprint lithography: methods and materials requirements, *Adv. Mater.*, **19**, pp. 495–513.
8. Kang, M.G., and Guo, L.J. (2007), Nanoimprinted semitransparent metal electrodes and their application in organic light-emitting diodes, *Adv. Mater.*, **19**, pp. 1391–1396.
9. Lee, J.H., Kim, C.H., Ho, K.M., and Constant, K. (2005), Two-polymer microtransfer moldings for highly layered microstructures, *Adv. Mater.*, **17**, pp. 2481–2485.
10. Chen, Y., and Goldman, A.M. (2008), A Simple approach to the formation of ultranarrow metal wires, *J. Appl. Phys.*, **103**, 054312 (4pp).

11. Chen, L., Wang, J.J., Walters, F., Deng, X., Buonanno, M., Tai, S., and Liu, X. (2007), Large flexible nanowire grid visible polarizer made by nanoimprint lithography, *Appl. Phys. Lett.*, **90**, 063111 (3pp).

12. Bai, J.G., Chang, C.L., Chung, J.H., and Lee, K.H. (2007), Shadow edge lithography for nanoscale patterning and manufacturing, *Nanotechnology*, **18**, 405307 (8pp).

13. Peng, Y., Cullis, T., and Inkson, B. (2008), Accurate electrical testing of individual gold nanowires by *in situ* scanning electron microscope nanomanipulators, *Appl. Phys. Lett.*, **93**, 183112 (3pp).

14. Wu, Y., Xiang, J., Yang, C., Lu, W., and Lieber, C.M. (2004), Single-crystal metallic nanowires and metal/semiconductor nanowire heterostructures, *Nature*, **430**, pp. 61–65.

15. Wu, B., Heidelberg, A., and Boland, J.J. (2005), Mechanical properties of ultra-high strength gold nanowires, *Nat. Mater.*, **4**, pp. 525–529.

16. Xiang, C., Kung, S.C., Taggart, D.K., Yang, F., Thompson, M.A., Guell, A.G., Yang, Y., and Penner, R.M. (2008), Lithographyically patterned nanowire electrodeposition: a method for patterning electrically continuous metal nanowires on dielectrics, *ACS Nano*, **2**, pp. 1939–1949.